Effects of Multibranching on 3-Hydroxyflavone-Based Chromophores and the Excited-State Intramolecular Proton Transfer Dynamics

Chao-Chen Lin, Chyi-Lin Chen, Min-Wen Chung, Yi-Ju Chen, and Pi-Tai Chou*

Department of Chemistry, National Taiwan University, No. 1, Section 4, Roosevelt Road, Taipei 10617, Taiwan, R.O.C.

Received: June 16, 2010; Revised Manuscript Received: August 12, 2010

A series of one-, two-, and three-branched chromophores based on 3-hydroxyflavones (**1**−**3**) have been synthesized as the first example of multibranched chromophores demonstrating excited-state intramolecular proton transfer (ESIPT). Coupling between the 3-hydroxyflavone branches connected by an electron-donating triphenylamine core is manifested in the red-shifted and asymmetric absorption band of **2**, whereas the absorption of **3** is governed by the divided donor strength. Their excited-state charge-transfer (ESCT)-coupled ESIPT dynamics is investigated via femtosecond fluorescence upconversion and is proved to be well correlated with the ratio of normal/tautomer emission in the fluorescence spectra. For **1** and **2**, with increased donor strength compared with the 4′-*N*,*N*-dialkylamino-3-hydroxyflavone analogue, ESIPT appears to cease in the more polar solvent of acetonitrile. Nevertheless, similar dependence of **1**−**3** on solvent polarity signifies resembling charge-transfer character at the normal excited states (N*), despite their varying structures. As evidenced by the theoretical approach, the frontier orbitals of vibrationally relaxed (geometry-optimized) N*, from which fluorescence and ESIPT should take place, are localized on one specific branch, leading to similar emission patterns and dynamics, whereas the orbitals contributing to Franck−Condon excitation (absorption) spread over the entire molecule. The localization is found to be facilitated by rotation of a specific branch pivoting on the central nitrogen atom, while planarity is maintained within each 3-hydroxyflavone chromophore.

1. Introduction

3-Hydroxyflavone has long been a prototypical case of excited-state intramolecular proton transfer (ESIPT).[1] Upon $S_0 \rightarrow S_1$ ($\pi\pi^*$) excitation (λ_{max} ∼340 nm in cyclohexane), ultrafast ESIPT is executed (<100 fs), resulting in the steady-state observation of only a largely Stokes-shifted tautomer emission band. Substitution at the 4′ position with a dialkylamino group renders an ideal example for studying excited-state charge-transfer (ESCT)-coupled ESIPT,[2,3] along with other systems, such as 7-*N*,*N*-diethylamino-3-hydroxyflavone[4] and *p*-*N*,*N*-ditolylaminosalicylaldehyde.[5] The amino group serves as an electron donor, of which the lone pair electrons can be viewed as being resonated to the carbonyl oxygen upon optical excitation, creating a large dipole moment for the normal excited state (N*) relative to the tautomer excited state (T*) and their respective ground states (N and T). From the theoretical work of Hynes and co-workers,[6] equilibrium between the moving proton and the surrounding solvent molecules is established at any instant so that the reaction activation energy ($\Delta G^{\dagger}$) is determined by solvent reorganization rather than a proton migration barrier and, hence, the adoption of solvent orientation (polarization) instead of proton position as the primary reaction coordinate. Moreover, N* is stabilized more as the solvent polarity is increased, thereby forming a larger solvent-induced barrier. For example, the barrier of 4′-*N*,*N*-dimethylamino-3-hydroxyflavone in dichloromethane is estimated to be 4.6 kcal/mol.[7] Even more intriguingly, it is discovered via the analysis of temporal spectral evolution within 3 ps that during solvent relaxation (SR) of N* toward N^*_{eq} (the equilibrium configuration), a competing ESIPT process takes place.[3] The feature can be attributed to the resembling dipolar vectors of T* and N in both magnitude and orientation (15°) such that prior to complete solvent relaxation (reorientation) to N^*_{eq}, the molecule undergoes a possibly adiabatic type of proton transfer (∼1.5 ps) in the absence of a solvent-induced barrier (Scheme 1).[3] It is also noteworthy that recent experimental advances in excited-state intramolecular proton-coupled electron transfer (PCET) reactions have been reviewed by Hsieh et al.[8]

In continuation of the effort, substitution at the 4′ position is further replaced with the diphenyl amino group (**1**), in hopes of increasing the donor strength. In the meantime, the resulting segment of a triphenylamine moiety suffices for an electron donor that has been used extensively as a building block for multibranched and dendritic structures.[9−11] On the basis of the triphenylamine donor core and the dipolar nature of 4′-*N*,*N*-diphenylamino-3-hydroxyflavone, the corresponding series of two- (V-shaped) and three-branched (trigonal) quadrupolar and octupolar molecules are crafted (**2** and **3**; see Scheme 2) to explore the effect of branching on steady-state spectra as well as on the ESIPT dynamics. Throughout this study, the electronic coupling between branches can be clearly resolved in the absorption spectra of **2** and **3**.

More significantly, as we demonstrate for the first time the integration of ESIPT into multibranched chromophores, the emission spectra and related dynamics are studied in various solvents to illustrate the impact of solvent polarity on the ESIPT rate. Similar solvent-dependent behavior indicates that the normal excited states (N*), where proton transfer is initiated,

* Corresponding author. E-mail: chop@ntu.edu.tw.

10.1021/jp105542z
Published on Web 09/07/2010

SCHEME 1: The Proposed Relaxation Mechanism[a] of 4′-*N*,*N*-Dialkylamino-3-hydroxyflavone in Polar Solvents[a]

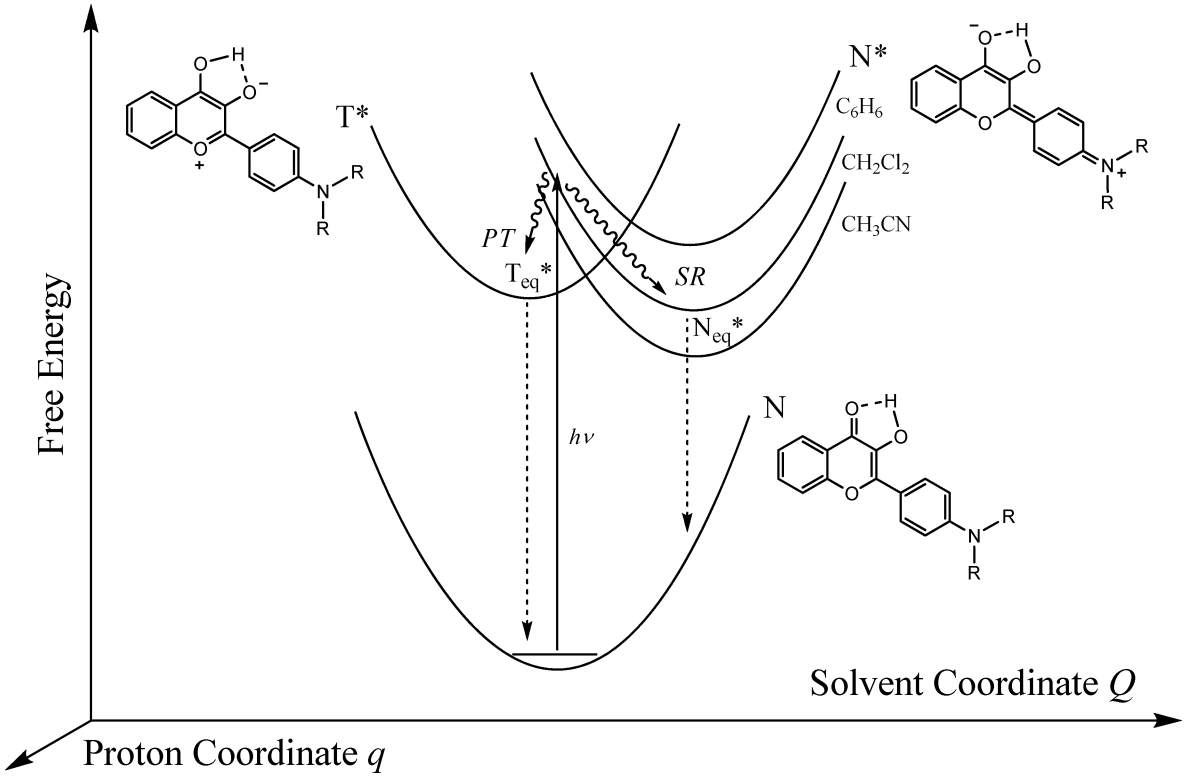

[a] See text for the definition of states and relaxation processes. Also note that a pyrylium cationic structure is commonly drawn for the 3-hydroxyflavone tautomer.

SCHEME 2: Synthesis of Compounds 1−3

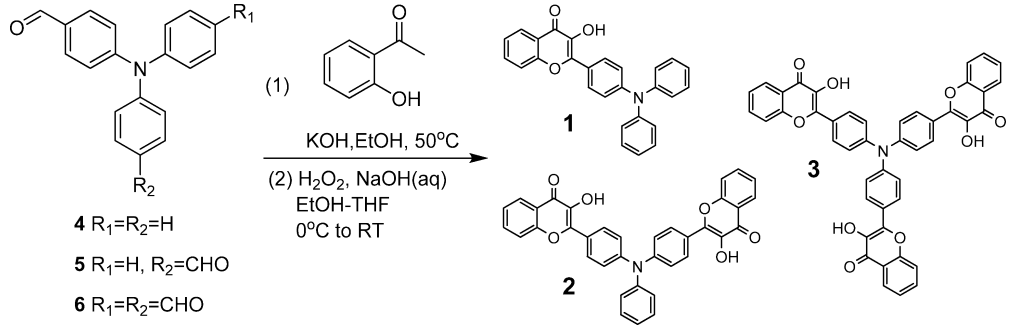

possess comparable dipolar vectors, despite the varying structures. It has been elucidated with quantum-chemical excited-state calculations that geometry optimization gives rise to the localization of frontier orbitals on one branch rather than being delocalized over the entire molecule.[9] Compared to multi-branched chromophores incorporating *trans*-stilbene linkage, which is intrinsically twisted at the ground state,[9,10a,c,e] through the utilization of compact planar 3-hydroxyflavone moieties, it is revealed that rotation of a whole single branch during vibrational relaxation causes the localization of emission chromophore.

2. Experimental Section

2.1. Synthesis. Scheme 2 depicts the synthetic procedures for compounds **1**−**3**, in which the first step involved the formation of chalcones via Claisen−Schmidt condensation[12] of commercially available compounds **4**, **5**, and **6** with *o*-hydroxyacetophenone (1.05 equiv, 6 mL/mmol acetophenone) in a mixture of 25 mL of dried EtOH and 5 mL of 50% aqueous KOH solution (2.9 equiv). The mixture was stirred at 50 °C for 3 h, cooled to room temperature, and then stayed overnight. The obtained chalcone salts were poured into water and neutralized to pH 6−7 with 1 M HCl; and the precipitates, which could be crystallized in EtOH, were subsequently filtered, washed with EtOH, and dried. Second, oxidative cyclization was conducted with addition to aqueous 30% H_2O_2 (8−11 equiv) and 4 M NaOH (5.0 equiv) in a 1:1 mixture of EtOH and THF (20 mL/mmol chalcone) at 0 °C. The reaction mixture was stirred at room temperature overnight, then acidified again with 1 M aqueous HCl and filtered off to yield the corresponding chromones **1**−**3**.

All reactions were performed under nitrogen. Solvents were distilled from appropriate drying agents prior to use. Commercially available reagents were used without further purification. All reactions were monitored by TLC with Merck precoated glass plates (0.20 mm with fluorescent indicator UV254) and were visualized with UV light irradiation at 254/366 nm. Flash column chromatography was carried out using

silica gel from Merck (230−400 mesh). The ^{1}H and ^{13}C NMR spectra were obtained on a 400 MHz Bruker spectrometer, and the chemical shifts were reported relative to $CDCl_3$. Mass spectra were obtained on a JEOL SX-102A instrument operating in electron impact (EI) mode. Elementary analyses were performed on a CHN analyzer.

2-(4-(Diphenylamino)phenyl)-3-hydroxy-4H-chromen-4-one (1). ^{1}H NMR δ 8.23−8.20 (dd, J = 21 Hz, 1H), 8.12−8.09 (m, 2H), 7.68−7.63(m, 1H), 7.54−7.52(d, J = 21 Hz, 1H), 7.40−7.36 (m, 1H), 7.31−7.27 (m, 4H), 7.16−7.07 (m, 8H). ^{13}C NMR: δ 172.7, 146.6, 137.5, 133.1, 129.5, 129.3, 128.9, 126.1, 125.4, 125.2, 124.2, 124.0, 123.3, 122.0, 121.0, 119.2, 118.0. EI-MS (MH^+): 406.14. Anal. Calcd for $C_{27}H_{19}NO_3$: C, 79.98; H, 4.72; N, 3.45; O, 11.84. Found: C, 79.95; H, 4.70; N, 3.47; O, 11.81.

2,2′-(4,4′-(Phenylazanediyl)bis(4,1-phenylene))bis(3-hydroxy-4H-chromen-4-one) (2). ^{1}H NMR δ 8.24−8.22 (d, J = 21 Hz, 2H), 8.18−8.16 (m, 4H), 7.69−7.66 (m, 2H), 7.56−7.54 (d, J = 21 Hz, 2H), 7.41−7.33 (m, 4H), 7.26−7.17 (m, 4H), 6.99 (br, 3H). ^{13}C NMR: δ 172.8, 155.1, 148.4, 143.1, 137.7, 133.3, 131.6, 129.6, 128.8, 126.1, 125.3, 124.9, 124.3, 123.5, 122.8, 120.6, 118.0. EI-MS (MH^+): 566.15. Anal. Calcd for $C_{36}H_{23}NO_6$: C, 76.45; H, 4.10; N, 2.48; O, 16.97. Found: C, 76.48; H, 4.12; N, 2.42; O, 16.93.

2,2′,2″-(4,4′,4″-Nitrilotris(benzene-4,1-diyl))tris(3-hydroxy-4H-chromen-4-one) (3). ^{1}H NMR δ 8.27−8.23 (m, 6H), 7.81−7.79 (d, J = 22 Hz, 3H), 7.71−7.58 (m, 3H), 7.45−7.41 (m, 3H), 7.36−7.28 (m, 6H). ^{13}C NMR: δ 172.6, 155.3, 133.6, 131.3, 129.2, 128.9, 125.5, 124.9, 124.5, 123.6, 122.6, 120.6, 118.1. EI-MS (MH^+): 725.16. Anal. Calcd for $C_{45}H_{27}NO_9$: C, 74.58; H, 3.62; N, 1.93; O, 19.87; Found: C, 74.57; H, 3.60; N, 1.92; O, 19.85.

2.2. Spectroscopic Measurements. Steady-state absorption and emission spectra were recorded by a Hitachi (U-3310) spectrophotometer and an Edinburgh (FS920) fluorometer, respectively, for which the wavelength-dependent response had been corrected. Nanosecond lifetime studies were performed with an Edinburgh FL 900 photon-counting system equipped with a hydrogen-filled lamp as the excitation source. Coumarin 480 (λ_{em} = 471 nm, Exciton) in ethanol, with a Φ of 0.95, served as the reference for measuring emission quantum yields.[13a] Emission quantum yields were calculated using

$$\Phi_s = \Phi_r \frac{I_s}{I_r}\frac{A_r}{A_s}\frac{{n_s}^2}{{n_r}^2} \quad (1)$$

by comparing the integrated areas (I, where the subscripts s and r denote sample and reference, respectively) under the fluorescence curves with similar absorbance (A) at the same excitation wavelength and were corrected for the refractive indices (n) of the solvents used.[13b]

The fluorescence upconversion measurements were performed using a femtosecond optically gated system (FOG-100, CDP), details of which have been described in previous reports.[14] Briefly, the fundamental of a Ti:sapphire laser (Tsunami, Spectra Physics) at 800 nm was used to produce second harmonics (SH) as the excitation source. The resulting fluorescence and the optical delayed remaining fundamental pulses were collected and focused on a BBO type-I crystal (0.5 mm) for sum-frequency generation. The upconverted signal was then separated by an F/4.9 (f = 380 mm) monochromator and detected via a photon-counting PMT (R1527P, Hamamatsu). The cross-correlation between SH and the fundamental had a full width at half-maximum (fwhm) of ∼150 fs, which was chosen as a response function of the system. A waveplate was placed in the pump beam path to ensure that the polarization was set at the magic angle (54.7°) with respect to that of the gate pulse to eliminate fluorescence anisotropy.

2.3. Computational Methodology. Ground-state and the lowest singlet excited-state (S_1) geometries were optimized by density functional theory (DFT) and analytic time-dependent DFT (TDDFT)[15] with the B3LYP[16] hybrid functional, which allows for DFT-quality optimizations in the excited state. The 6-31G(d)[17] basis set was employed for all atoms. Vibrational frequencies were then calculated on the basis of their optimized geometries to verify that each of the calculated geometies is the globally optimized structure. Time-dependent DFT (TD-DFT)[18] calculations using the B3LYP functional were then performed on the basis of the optimized structures at ground states to probe the absorptive properties. Typically, the lowest 10 singlet roots of the nonhermitian eigenvalue equations were obtained to determine the vertical excitation energies. Oscillator strengths were deduced from the dipole transition matrix elements. All calculations were carried out using Gaussian 09 program.[19]

3. Results and Discussion

3.1. Steady-State Absorption Spectra. The steady-state absorption spectra of compounds **1**−**3** in various solvents are shown in Figure 1, and the extinction coefficients in dichloromethane are plotted in Figure 2. Considering the low ionization energy for the amino substituent, the $S_0 \rightarrow S_1$ excitation of **1** should be ascribed to the charge-transfer transition from diphenylamine (electron donor) to the carbonyl oxygen (electron acceptor).[3] Vibronic structure is observed in cyclohexane, conveying that the charge-transfer transition is $\pi\pi^*$ by nature, as in the parent 3-hydroxyflavone molecule.

Meanwhile, in polar solvents, the vibronic feature is concealed by inhomogeneous broadening. Going from **1** to **3**, extinction coefficients at the first absorption peak (ε_{max}; see Table 1) in dichloromethane are in the ratio of 1.0:1.8:2.4, which is not strictly proportional to the number of branches, implying that upon absorption, the transitions are delocalized among branches for **2** and **3**. The delocalization, or coupling of branching chromophores, is also evident in the peak wavelength and shape of the lowest energy absorption bands for **2**. Obviously, the first absorption peak (λ_{max}) of **2** (429 nm) is red-shifted from that of **1** (404 nm), which is attributed to coupling between the S_1 states of each separate branch, resulting in one stabilized and one destabilized state. These states eventually become the new S_1 (represented as S_1') and S_2', being slightly higher in energy (vide infra). Moreover, the observed absorption band of **2** is distinctively asymmetric owing to the differing transition dipole moments of S_1' and S_2'.[9] This viewpoint can be supported by the computed oscillator strengths listed in Table 2 (f = 0.93 and 0.18 for S_1' and S_2', respectively).

In stark contrast, λ_{max} of **3** is blue-shifted to 396 nm, suggesting that multibranching leads to not only coupling between states but also other effects. Since for 4′-*N*,*N*-dialkylamino-3-hydroxyflavone or **1**, the HOMO resides at the amino group, as multibranching is introduced, the donating strength is divided, and the HOMO energy level should be lowered, resulting in a larger S_0-S_1 energy gap. Therefore, multibranching introduces two opposing effects; that is, splitting of energy levels, which decreases the S_0-S_1 energy gap; and weakening of the donor strength, which increases the S_0-S_1 energy gap. The impact of weakened donor strength should be

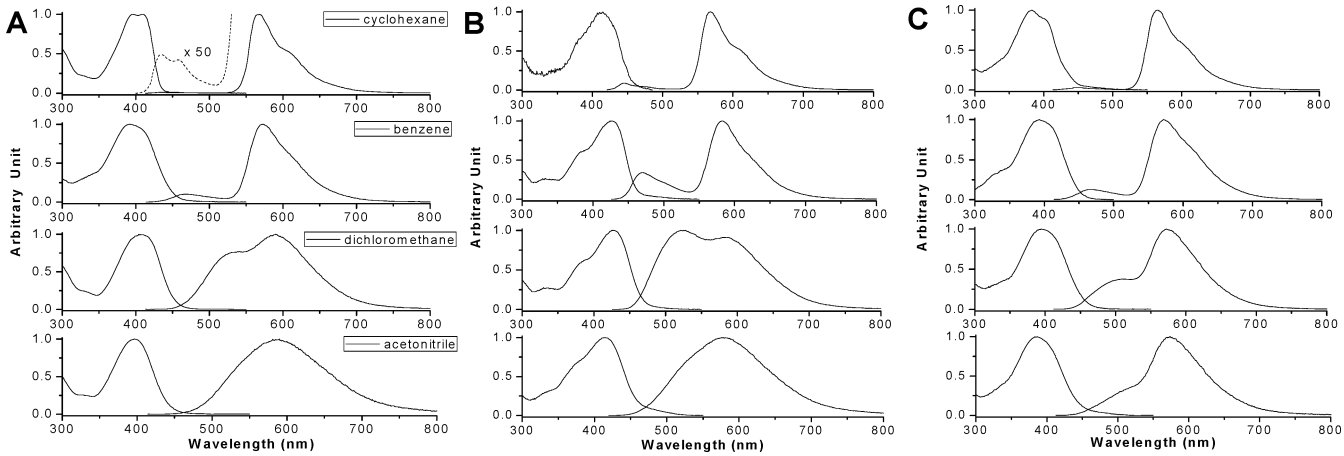

Figure 1. Static absorption and fluorescence spectra of (A) **1**, (B) **2**, and (C) **3** in cyclohexane, benzene, dichloromethane, and acetonitrile at 298 K.

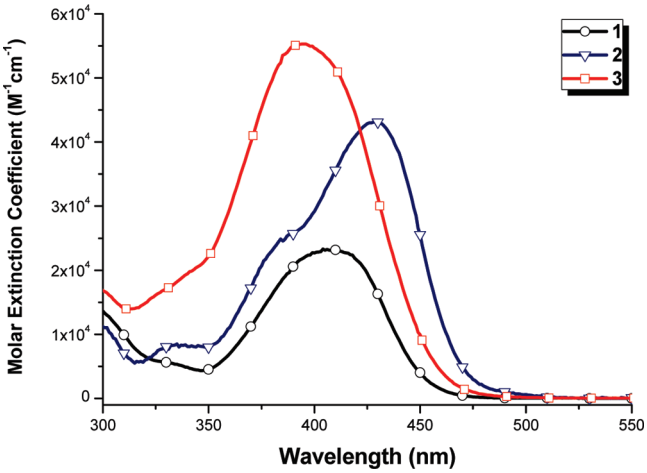

Figure 2. Molar extinction coefficients of compounds **1**−**3** in dichloromethane.

TABLE 1: Absorption Properties of Compounds 1−3 in Dichloromethane

	λ_{max} (nm)	ε_{max} (M^{-1} cm^{-1})
1	404	2.33×10^4
2	429	4.32×10^4
3	396	5.53×10^4

TABLE 2: Calculated Energy Levels, Oscillator Strengths (*f*), and Orbital Transition Analyses of Lower-Lying Transitions (Absorption) for Compounds 1−3

	state	λ_{cal} (nm)[a]	f[b]	assignments
1	S_1	431.1	0.6465	HOMO → LUMO (99%)
2	S_1'	462.6	0.9256	HOMO → LUMO (99%)
	S_2'	421.3	0.1793	HOMO → LUMO+1 (97%)
3	S_1''	468.6	0.7507	HOMO → LUMO (97%)
	S_2''	466.9	0.7582	HOMO → LUMO+1 (97%)
	S_3''	411.4	0.0007	HOMO → LUMO+2 (95%)

[a] Calculated absorption onset. [b] Oscillator Strength.

more prominent in our case of compounds **1**−**3** because of the planarity and, hence, better electron-withdrawing ability through the intact conjugation of each branch (Figure 3); that is, the 3-hydroxyflavone chromophore. With the triphenylamine core, **1**−**3** all exhibit propeller-like geometry, in which each branch is twisted with respect to the plane defined by the central nitrogen atom and the three connecting carbons, whereas each

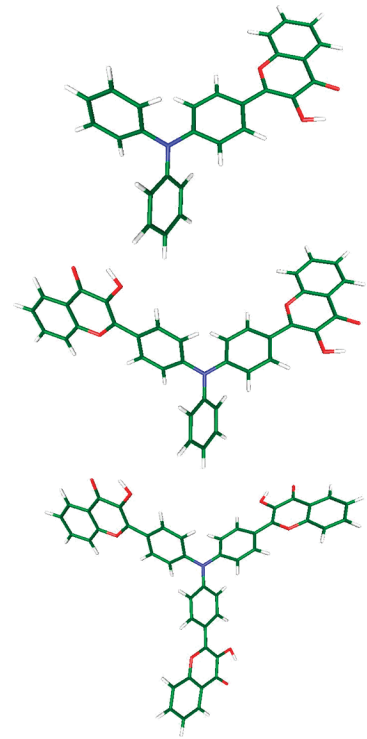

Figure 3. Optimized ground state geometry of compounds **1**−**3**.

dipolar branch maintains planarity in **2** and **3**. The intact 3-hydroxyflavone chromophore with dihedral angle between the phenyl group and the chromenone moiety of <0.5°, compared with nonplanar (twisted) branches,[9,10] raises the S_1 energy of **3** (represented as S_1'') to an extent that trumps the stabilizing interaction due to coupling between S_1 states on each branch. Conversely, the latter effect dominates in **2**. It is also worthy to note that this trend is not reflected in the calculated absorption wavelength (λ_{cal}) using TDDFT (Table 2). Nevertheless, it can be seen that the coupling effect is less obvious going from **2** to **3**. On the other hand, coupling among branches in **3** produces two degenerate lowest-lying states, S_1'', with $f = 0.75$ and S_2'' with $f = 0.76$, and one higher lying state, S_3'' with vanishing oscillator strength ($f = 0.0007$).[9] Thus, the observed first absorption band of **3** returns to being symmetric, as opposed to that of **2**, indicative of a 3-fold symmetry axis.

TABLE 3: Emission and Relaxation Dynamics of Compounds 1−3 in Selected Solvents

	solvent	emission λ_{max} (Φ)	early dynamics (ps)[a]	population decay (ns)
1	cyclohexane	N: 434 nm (0.0070)	480 nm [τ_1: 7.67 (0.98)]	2.96
		T: 568 nm (0.52)	650 nm [τ_1: 7.28 (−0.55)]	
	benzene	N: 467 nm (0.039)	480 nm [τ_1: 23.3 (0.99)]	2.89
		T: 572 nm (0.52)	650 nm [τ_1: 23.9 (−0.46)]	
	dichloromethane	N: 513 nm (0.11)	480 nm [τ_1: 3.18 (0.69), τ_2: 97.1 (0.30)]	3.56
		T: 589 nm (0.54)	650 nm [τ_1: 2.94 (−0.19), τ_2: 98.5 (−0.22)]	
	acetonitrile	N: 590 nm (0.14)	480 nm [τ_1: 0.96 (0.92)]	1.44
			650 nm [τ_1: 0.51 (−0.50)]	
2	cyclohexane	N: 444 nm (0.052)	480 nm [τ_1: 13.7 (0.85)]	3.02
		T: 568 nm (0.49)		
	dichloromethane	N: 513 nm (0.18)	480 nm [τ_1: 2.48 (0.85), τ_2: 259 (0.10)]	2.94
		T: 583 nm (0.44)		
3	cyclohexane	N: 448 nm (0.018)	480 nm [τ_1: 10.1 (0.88)]	3.35
		T: 565 nm (0.52)		
	dichloromethane	N: 484 nm (0.12)	480 nm [τ_1: 1.57 (0.51), τ_2: 88.3 (0.37)]	2.89
		T: 581 nm (0.52)		

[a] Numbers in parentheses are the fitted preexponential factors, with negative values indicating rise time constants. Note that the sum of preexponential factors may not be equal to 1 due to exclusion of the longer population decay component.

3.2. Fluorescence Spectra and Femto−Picosecond Relaxation Dynamics. Fluorescence spectra of compounds **1**−**3** are depicted in Figure 1, and the relevant data as well as detailed fitting parameters for relaxation dynamics are listed in Table 3. In cyclohexane, largely Stokes-shifted tautomer emission centering around 570 nm predominates, and the charge-transfer normal emission around 440 nm is still visible, implying fast but finite ESIPT in nonpolar solvent. The emission quantum yields of all compounds (e.g., $\Phi = 0.52$ for **1** in cyclohexane) are more than twice the value of 4′-*N*,*N*-diethylamino-3-hydroxyflavone (e.g., $\Phi = 0.21$ in cyclohexane),[3] accompanied by longer population decay times; for instance, 2.96 ns for **1** relative to 1.28 ns for 4′-*N*,*N*-diethylamino-3-hydroxyflavone in cyclohexane. This enhancement can be rationalized with suppressed rotation of the phenyl rings caused by steric hindrance and thus a reduced nonradiative decay rate (k_{nr}), whereas the motions of flexible alkyl groups channel into nonradiative deactivation.

Take **1** as a prototype, when the solvent polarity is increased, the ratio of normal emission increases correspondingly and shifts to longer wavelength, until in acetonitrile, only one emission band remains. Supposedly, ESIPT does not occur in acetonitrile for **1**, which can be confirmed with the absence of proton transfer dynamics in addition to solvent relaxation (SR) and the population decay (vide infra). With femtosecond fluorescence upconversion, the dynamics of normal emission at 480 nm for **1** in cyclohexane (Figure 4) is determined to be composed of a 7.67 ps fast decay (98%) and a residual long-lived component.

On the other hand, the tautomer emission dynamics at 650 nm consists of a 7.28 ps rise time constant (−55%) plus a long population decay. After acquiring the population decays, it is found that the two time constants (τ_1 and the population decay) for tautomer emission resemble those of normal emission within experimental error. Bringing in the fact that the magnitudes of the two pre-exponential factors for the tautomer emission are roughly the same, **1** follows the same kinetic model as 4′-*N*,*N*-dialkylamino-3-hydroxyflavone,[2,3] in which fast equilibrium is established between normal (N*) and tautomer (T*) excited states in more polar solvents, such as dichloromethane and acetonitrile. The associated kinetics for [N*] and [T*] are outlined as follows.

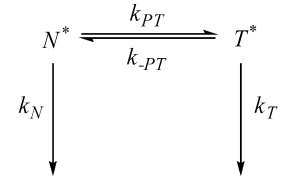

(2)

$$[N^*(t)] = [N^*(0)]\left(B_1 e^{-t/\tau_1} + B_2 e^{-t/\tau_2}\right)$$
$$[T^*(t)] = [N^*(0)]B_1\left(-e^{-t/\tau_1} + e^{-t/\tau_2}\right) \quad (3)$$

$$\frac{1}{\tau_1} = k_1 \cong k_{PT} + k_{-PT}$$
$$\frac{1}{\tau_2} = k_2 = k_T\left(\frac{k_{PT}}{k_{PT} + k_{-PT}}\right) + k_N\left(\frac{k_{-PT}}{k_{PT} + k_{-PT}}\right) \quad (4)$$

$$B_1 \cong \frac{k_{PT}}{k_{PT} + k_{-PT}}$$
$$B_2 \cong \frac{k_{-PT}}{k_{PT} + k_{-PT}} \quad (5)$$

The relations hold true if the forward and reverse rates of ESIPT, k_{PT} and k_{-PT}, are much faster than the population decay rates for both states, k_N and k_T. The same phenomenon is observed in benzene for **1**, with a 23.3 ps fast decay (99%) at 480 nm normal emission and a correlated 23.9 ps rise (−46%) at 650 nm tautomer emission, plus similar population decays for the two bands. Nonetheless, k_{-PT} for **1** in both cyclohexane and benzene is relatively slow compared to k_{PT} so that B_2 (see eq 5) is minute (Table 3).

Relaxation dynamics in dichloromethane is drastically different in that at least three time constants are apparently needed (Figure 4) to achieve good convoluted fits. For example, upon monitoring at the 480 nm normal emission of **1**, two fast decays, $\tau_1 = 3.18$ ps (69%) and $\tau_2 = 97.1$ ps (30%), are resolved in

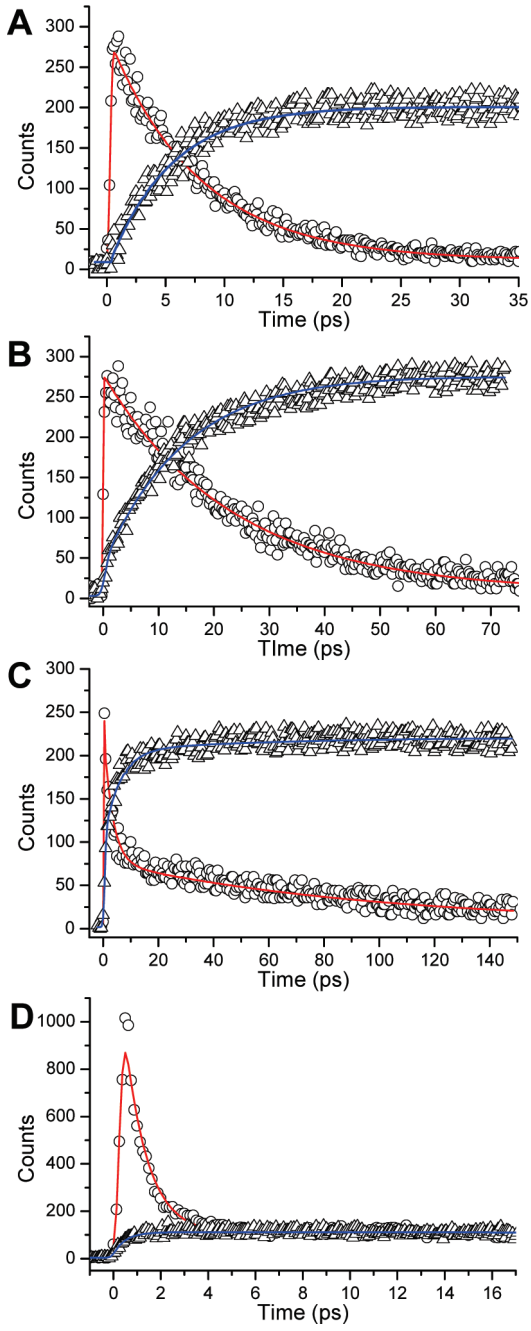

Figure 4. Time-resolved sum frequency signal of fluorescence at (o) 480 and (Δ) 650 nm with the gate pulse (800 nm) for **1** in (A) cyclohexane, (B) benzene, (C) dichloromethane, and (D) acetonitrile. Solid lines are the best-fitting curves.

addition to the longer population decay, with τ_1 ascribed to SR and τ_2 to ESIPT. Solvent relaxation is definitely expected for N* owing to its significant charge separation. Interestingly, two rises with similar time scales, $\tau_1 = 2.94$ ps (−19%) and $\tau_2 =$ 98.5 ps (−22%) are obtained at 650 nm tautomer emission, even though the dipole moment of T* was estimated to be somewhat smaller.[3]

Through analysis of the temporal spectral evolution of 4′-*N*,*N*-diethylamino-3-hydroxyflavone,[3] it was discovered that the tautomer emission band emerged alongside the continuously red-shifting charge-transfer normal emission band within ∼1 ps, hinting an ESIPT pathway that is occurring simultaneously with solvent relaxation. This ultrafast ESIPT process is promoted by similar dipolar vectors of the tautomer excited state (T*) and the normal form ground state (N). Accordingly, at early times subsequent to excitation, the solvent orientation (polarization) remains favorable for N and T*, allowing execution of ultrafast ESIPT prior to the formation of a solvent-induced barrier. At times later than 30 ps, when solvent relaxation is nearly complete, the spectral feature displays a decrease in normal emission and an increase in tautomer emission, which can be rationalized by the slower ESIPT rate due to different polarizations between equilibrated normal (N^*_{eq}) and tautomer (T^*_{eq}) excited states (Scheme 1) and the existence of a solvent-induced barrier.

The most significant distinction between **1** and 4′-*N*,*N*-diethylamino-3-hydroxyflavone lies in that only one emission band exists in acetonitrile for **1**, presumably the normal emission, signifying the prohibition of ESIPT. This conclusion is validated with the observations of ultrafast solvent relaxation (e.g. 0.96 ps decay at 480 nm versus 0.51 ps rise at 650 nm) and population decay (1.44 ns) only, with no intermediate kinetic processes. Such results act in accordance with the increased donating strength of $-NPh_2$ relative to $-NR_2$, which on one hand creates a larger dipole moment in the charge-transfer normal excited state (N*), shifting the equilibrium position of N^*_{eq} farther away from that of T^*_{eq} and in turn resulting in a larger solvent induced barrier, so that the rate of ESIPT could not compete with other relaxation pathways of N*.[8,20]

Alternatively, it may indicate that N* of **1** is stabilized more than its dialkylamino analogue, such that N^*_{eq} is much lower in energy than T^*_{eq}, leading to thermally unfavorable $N^*_{eq} \rightarrow T^*_{eq}$ ESIPT. Note that the prohibition of ESIPT is also observed for **2** in acetonitrile. Nevertheless, ESIPT recovers for **3** in acetonitrile, which is supported by the steady-state observation of dual emission, indirectly hinting the greater influence of weakened donor strength in **3** due to multibranching, as proposed in earlier sections.

Last but not least, the dynamics inspected with fluorescence upconversion for the whole series of compounds **1**−**3** is always consistent with the steady-state measurements. In other words, a faster ESIPT rate is associated with a minor proportion of the normal emission. For instance, the ESIPT dynamics of **1**−**3** in cyclohexane (Figure 5) is on the order of **1** (7.67 ps^{-1}) > **3** (10.1 ps^{-1}) > **2** (13.7 ps^{-1}), with **1** having the smallest ratio of normal emission and **2** having the largest. In dichloromethane (Figure 6), ESIPT dynamics is **3** (88.3 ps^{-1}) > **1** (97.1 ps^{-1}) > **2** (259 ps^{-1}), consistent with the trend of an increasing normal emission ratio.

Overall, similar ESIPT behavior of **1**−**3** suggests that the normal excited states (N*) in which ESIPT originates possess analogous dipolar vectors. Nonetheless, this disagrees with the consequence of electronic coupling between branches in **2** and **3**, which may lead to cancellation of dipole moments owing to the relatively more symmetric V-shape and trigonal structures. To resolve this contradiction, theoretical approaches are then pursued to sort out how the delocalized Franck−Condon states (N^*_{FC}) of **1**−**3** generated upon absorption evolves into states with resembling dipolar vectors through vibrational relaxation.

3.3. Theoretical Approaches. The frontier orbitals of compounds **1**−**3** for absorption (Franck−Condon excitation) are calculated first with TDDFT and those of the lowest-lying excited states (S_1 for **1**, S_1' for **2**, and S_1'' for **3**; see Table 2) are illustrated in Figure 7. These states, in particular, can be well-represented as transitions between a pair of orbitals with >97% contribution. Delocalization among branches is unambiguous in **2** and **3**, with HOMO being located primarily around the

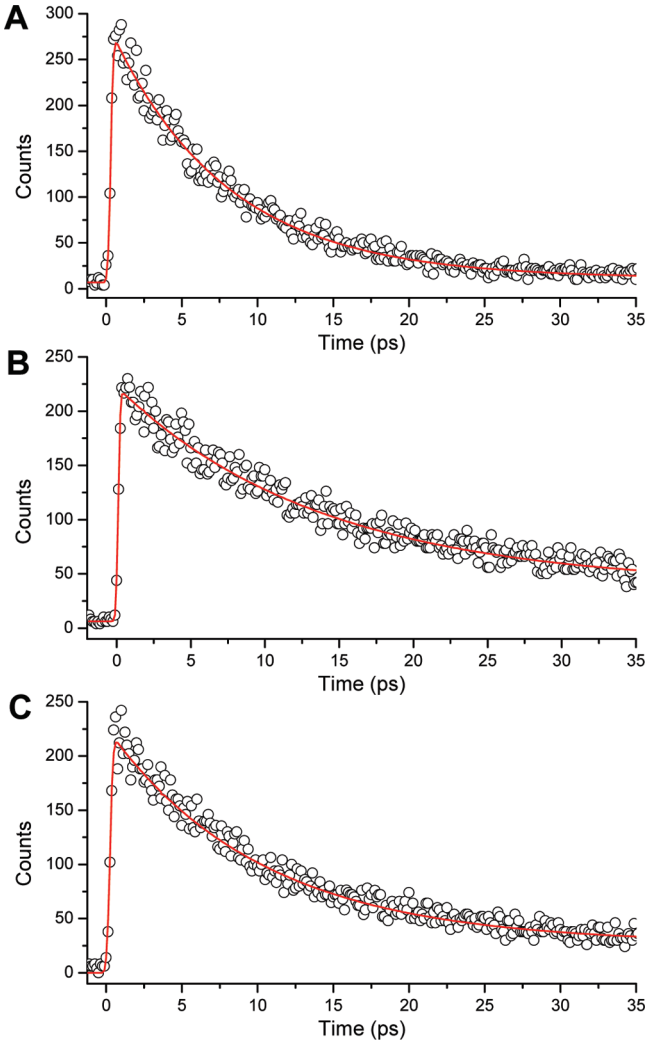

Figure 5. Time-resolved sum-frequency signal of fluorescence at 480 nm with the gate pulse (800 nm) for (A) **1**, (B) **2**, and (C) **3** in cyclohexane.

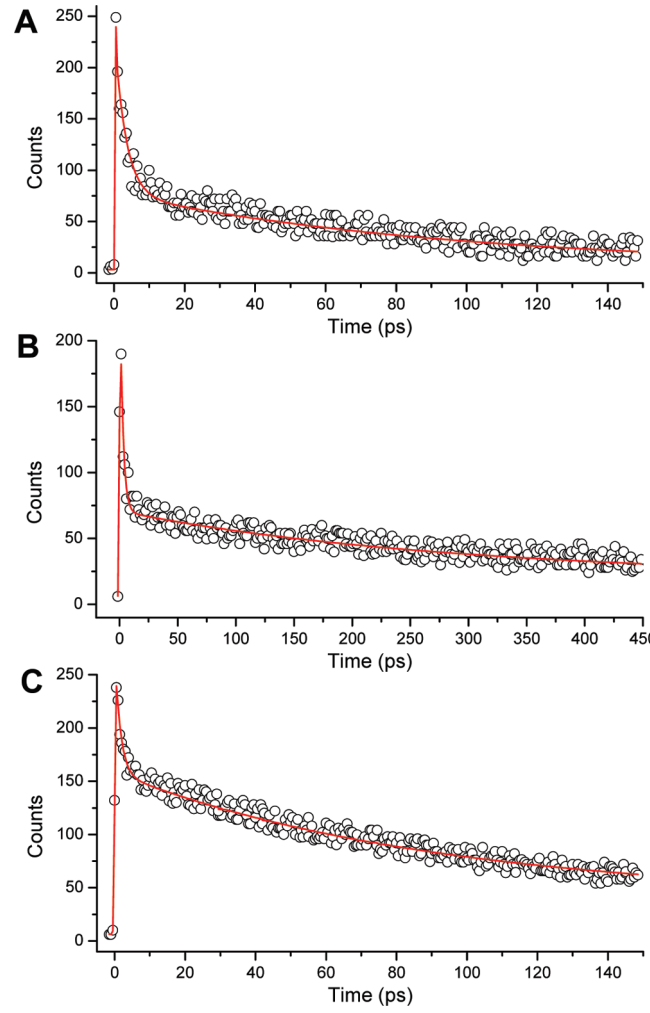

Figure 6. Time-resolved sum-frequency signal of fluorescence at 480 nm with the gate pulse (800 nm) for (A) **1**, (B) **2**, and (C) **3** in dichloromethane.

triphenylamine core and LUMO onto all of the 3-hydroxyflavone chromophores. For **3**, owing to degeneracy of the lowest-lying excited states, the LUMO should be a linear combination of two orbitals, each falling on two dipolar branches. On the other hand, after geometry optimization at S_1' and S_1'', designated as the emission states, in which ESIPT originates and competes with the normal emission, the frontier orbitals are found to be funneled into specific branches. The localization is a consequence of vibrational relaxation, which is also perceived in the Frenkel exciton model.[21] As a matter of fact, localized emitting states have been explored in several multibranched systems; for example, trigonal structures with triphenylamine or triphenylbenzene cores.[22]

In the case of **2** and **3**, vibrational relaxation is clearly manifested in the rotation of one single branch, with the electron configuration adjusting instantaneously such that LUMO resides solely on the rotated branch, while HOMO is on another unchanged branch including the central N atom. Presumably, in the emitting state, the nitrogen nonbonding orbital resonates efficiently only with the unchanged 3-hydroxyflavone chromophore, constituting an effective electron-donating segment.

In contrast, in the absorbing state, which adopts the optimized propeller-like geometry of the ground state (Figure 3), the nitrogen lone pair is equally shared by all branches. As a supplement, the dipole moments of the emitting states for **1**−**3** are superimposed in Figure 7, and their magnitudes are estimated to be 3.4, 6.8, and 5.9 D, respectively. With the dipolar vectors evidently not canceled out for **2** and **3** despite their symmetric structures, it is verified that similar solvent-dependent ESIPT is executed at the localized S_1 states created after vibrational relaxation.

4. Conclusion

In this work, we have successfully designed a series of one- (dipolar), two- (quadrupolar), and three-branched (octupolar) molecules **1**−**3** bearing triphenylamine as the electron donor core and 3-hydroxyflavone chromophores at the para positions as accepting branches. Akin to the previously studied 4′-*N*,*N*-dialkylamino-3-hydroxyflavone, excited-state charge-transfer coupled excited-state intramolecular proton transfer is demonstrated via emission spectra and the corresponding dynamics. When the solvent polarity is increased, the ESIPT rate decreases owing to a larger solvent-induced barrier. The initial 1−3 ps formation time of the tautomer emission observed in dichloromethane is facilitated by the resembling dipolar vectors of the normal form ground state (N) and the tautomer excited state (T*) before and during SR. In acetonitrile, the solvent-induced barrier is too large to allow for ESIPT in **1** and **2**, and only the normal emission bands are visible.

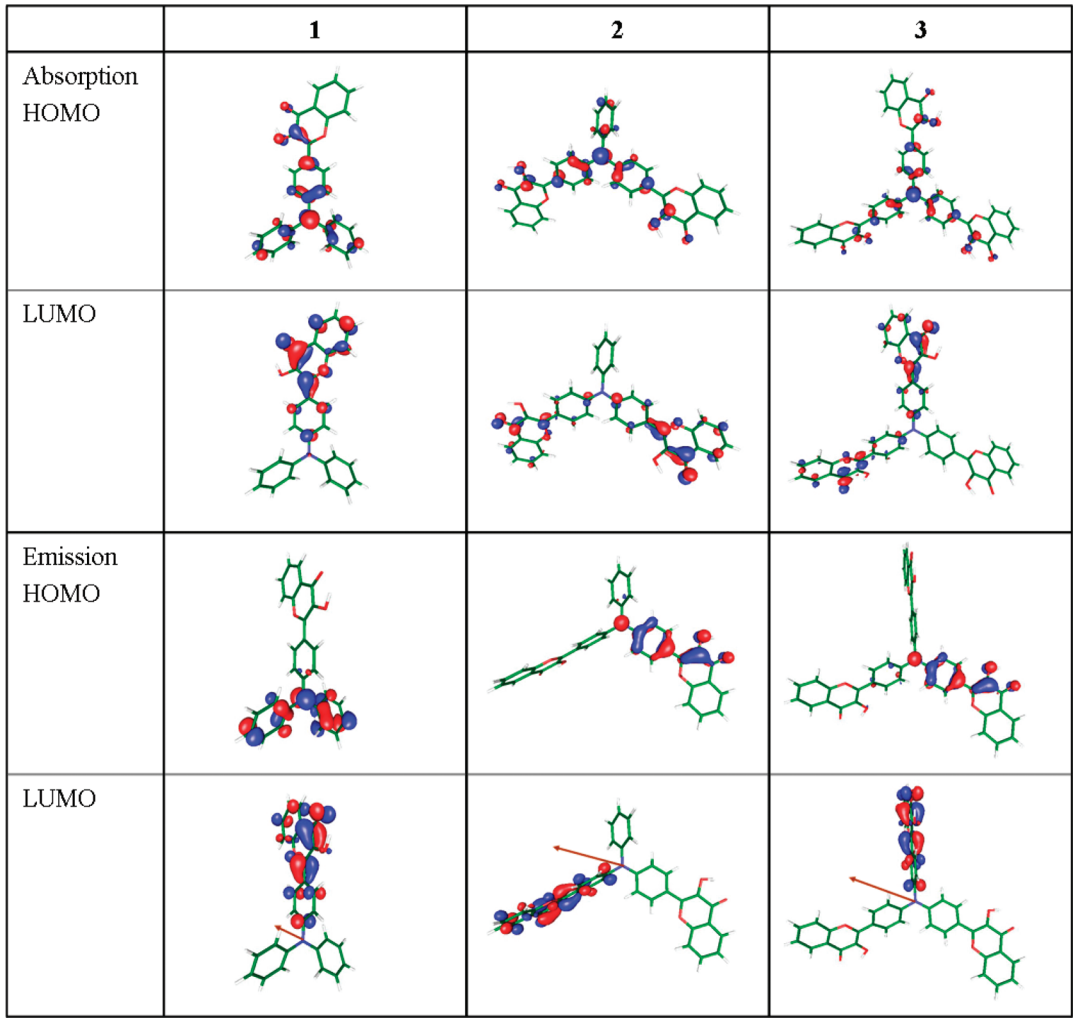

Figure 7. Frontier orbitals of compounds **1**−**3** for absorption and emission at the respective S_1 states. Brown arrows indicate dipolar vectors at the emission states.

Second, delocalization of excitation or electronic coupling between branches is clearly shown in the absorption spectra. Moreover, with theoretical approaches, it is revealed that upon vibrational relaxation at the S_1 states, rotation of one single branch fosters the localization of transition orbitals, with LUMO located merely on the rotated 3-hydroxyflavone chromophore and HOMO on another unchanged branch. This localization results in similar ESIPT behavior for **1**−**3** despite their differing structures. In view of the application, we have provided a new design strategy for quadrupolar or octupolar two-photon absorbing (TPA) chromophores, especially in the fields of two-photon imaging,[23,24] and the related TPA studies are currently in progress.

When branches capable of ESIPT are integrated, the interfering autofluorescence can be bypassed, since there is a large Stokes shift between the absorption and tautomer emission. If the conjugation is further elongated, the largely Stokes-shifted tautomer emission could even be tuned to near-infrared, providing better penetration without a large increase in molecular weight. Furthermore, via coupling with ESCT, emission spectra of the fabricated TPA chromophores are essentially sensitive to the local solvent polarity or hydrogen bonding environments, serving as prospective molecular probes.

Acknowledgment. We thank the National Science Council of Taiwan for financial support and the National Center for High-Performance Computing for computer time and facilities.

References and Notes

(1) (a) Sengupta, P.; Kasha, M. *Chem. Phys. Lett.* **1979**, *68*, 382. (b) Strandjord, A. J. G.; Courtney, S. H.; Friedrich, D. M.; Barbara, P. F. *J. Phys. Chem.* **1983**, *87*, 1125. (c) McMorrow, D.; Kasha, M. *J. Phys. Chem.* **1984**, *88*, 2235. (d) Schwartz, B. J.; Peteanu, L. A.; Harris, C. B. *J. Phys. Chem.* **1992**, *86*, 3591. (e) Ameer-Beg, S.; Ormson, S. M.; Brown, R. G.; Matousek, P.; Towrie, M.; Nibbering, E. T. J.; Foggi, P.; Neuwahl, F. V. R. *J. Phys. Chem. A* **2001**, *105*, 3709.

(2) (a) Shynkar, V. V.; Mély, Y.; Duportail, G.; Piémont, E.; Klymchenko, A. S.; Demchenko, A. P. *J. Phys. Chem. A* **2003**, *107*, 9522. (b) Swinney, T. C.; Kelley, D. F. *J. Chem. Phys.* **1993**, *99*, 211. (c) Douhal, A.; Sanz, M.; Carranza, M. A.; Organero, J. A.; Santos, L. *Chem. Phys. Lett.* **2004**, *394*, 54. (d) Ameer-Beg, S.; Ormson, S. M.; Poteau, X.; Brown, R. G.; Foggi, P.; Bussotti, L.; Neuwahl, F. V. R. *J. Phys. Chem. A* **2004**, *108*, 6938.

(3) Chou, P.-T.; Pu, S.-C.; Cheng, Y.-M.; Yu, W.-S.; Yu, Y.-C.; Hung, F.-T.; Hu, W.-P. *J. Phys. Chem. A* **2005**, *109*, 3777.

(4) Cheng, Y.-M.; Pu, S.-C.; Yu, Y.-C.; Chou, P.-T.; Huang, C.-H.; Chen, C.-T. *J. Phys. Chem. A* **2005**, *109*, 11696.

(5) Chou, P.-T.; Yu, W.-S.; Cheng, Y.-M.; Pu, S.-C.; Yu, Y.-C.; Lin, Y.-C.; Huang, C.-H.; Chen, C.-T. *J. Phys. Chem. A* **2004**, *108*, 6487.

(6) (a) Kiefer, P. M.; Hynes, J. T. *J. Phys. Chem. A* **2002**, *106*, 1834. (b) Kiefer, P. M.; Hynes, J. T. *J. Phys. Chem. A* **2002**, *106*, 1850.

(7) Roshal, A. D.; Organero, J. A.; Douhal, A. *Chem. Phys. Lett.* **2003**, *379*, 53.

(8) Hsieh, C.-C.; Jiang, C.-M.; Chou, P.-T. *Acc. Chem. Res.* **2010**, DOI: 10.1021/ar1000499.

(9) Katan, C.; Terenziani, F.; Mongin, O.; Werts, M. H. V.; Porrès, L.; Pons, T.; Mertz, J.; Tretiak, S.; Blanchard-Desce, M. *J. Phys. Chem. A* **2005**, *109*, 3024.

(10) (a) Chung, S.-J.; Kim, K.-S.; Lin, T.-C.; He, G. S.; Swiatkiewicz, J.; Prasad, P. N. *J. Phys. Chem. B* **1999**, *103*, 10741. (b) He, G. S.; Swiatkiewicz, J.; Jiang, Y.; Prasad, P. N.; Reinhardt, B. A.; Tan, L.-S.;

Kannan, R. *J. Phys. Chem. A* **2000**, *104*, 4805. (c) Porrès, L.; Mongin, O.; Katan, C.; Charlot, M.; Pons, T.; Mertz, J.; Blanchard-Desce, M. *Org. Lett.* **2004**, *6*, 47. (d) Yoo, J.; Yang, S. K.; Jeong, M.-Y.; Ahn, H. C.; Jeon, S.-J.; Cho, B. R. *Org. Lett.* **2003**, *5*, 645. (e) Kato, S.-i.; Matsumoto, T.; Shigeiwa, M.; Gorohmaru, H.; Maeda, S.; Ishi-i, T.; Mataka, S. *Chem.—Eur. J.* **2006**, *12*, 2303.

(11) (a) Drobizhev, M.; Karotki, A.; Rebane, A.; Spangler, C. W. *Opt. Lett.* **2001**, *26*, 1081. (b) Adronov, A.; Fréchet, J. M. J.; He, G. S.; Kim, K.-S.; Chung, S.-J.; Swiatkiewicz, J.; Prasad, P. N. *Chem. Mater.* **2000**, *12*, 2838. (c) Varnavski, O.; Yan, X.; Mongin, O.; Blanchard-Desce, M.; Goodson, T., III. *J. Phys. Chem. C* **2007**, *111*, 149.

(12) (a) Chou, P. T.; Martinez, M. L.; Clements, J. H. *J. Phys. Chem.* **1993**, *97*, 2618. (b) Chou, P. T.; Martinez, M. L.; Clements, J. H. *Chem. Phys. Lett.* **1993**, *204*, 395.

(13) (a) Jones, G.; Jackson, W. R.; Choi, C. Y.; Bergmark, W. R. *J. Phys. Chem.* **1985**, *89*, 294. (b) Lakowicz, J. R. *Principles of Fluorescence Spectroscopy*; Plenum Press: New York, 1983.

(14) (a) Chou, P. T.; Chen, Y. C.; Yu, W. S.; Chou, Y. H.; Wei, C. Y.; Cheng, Y. M. *J. Phys. Chem. A* **2001**, *105*, 1731. (b) Chou, P. T.; Yu, W. S.; Cheng, Y. M.; Pu, S. C.; Yu, Y. C.; Lin, Y. C.; Huang, C. H.; Chen, C. T. *J. Phys. Chem. A* **2004**, *108*, 6487.

(15) (a) Furche, F.; Ahlrichs, R. *J. Chem. Phys.* **2002**, *117*, 7433. (b) Scalmani, G.; Frisch, M. J.; Mennucci, B.; Tomasi, J.; Cammi, R.; Barone, V. *J. Chem. Phys.* **2006**, *124*, 094107, 1−15.

(16) (a) Lee, C.; Yang, W.; Parr, R. G. *Phys. Rev. B* **1988**, *37*, 785. (b) Becke, A. D. *J. Chem. Phys.* **1993**, *98*, 5648.

(17) Hariharan, P. C.; Pople, J. A. *Mol. Phys.* **1974**, *27*, 209.

(18) (a) Jamorski, C.; Casida, M. E.; Salahub, D. R. *J. Chem. Phys.* **1996**, *104*, 5134. (b) Petersilka, M.; Grossmann, U. J.; Gross, E. K. U. *Phys. Rev. Lett.* **1996**, *76*, 1212. (c) Bauernschmitt, R.; Ahlrichs, R.; Hennrich, F. H.; Kappes, M. M. *J. Am. Chem. Soc.* **1998**, *120*, 5052. (d) Casida, M. E. *J. Chem. Phys.* **1998**, *108*, 4439. (e) Stratmann, R. E.; Scuseria, G. E.; Frisch, M. J. *J. Chem. Phys.* **1998**, *109*, 8218.

(19) Frisch, M. J.; Trucks, G. W.; Schlegel, H. B.; Scuseria, G. E.; Robb, M. A.; Cheeseman, J. R.; Scalmani, G.; Barone, V.; Mennucci, B.; Petersson, G. A.; Nakatsuji, H.; Caricato, M.; Li, X.; Hratchian, H. P.; Izmaylov, A. F.; Bloino, J.; Zheng, G.; Sonnenberg, J. L.; Hada, M.; Ehara, M.; Toyota, K.; Fukuda, R.; Hasegawa, J.; Ishida, M.; Nakajima, T.; Honda, Y.; Kitao, O.; Nakai, H.; Vreven, T.; Montgomery, J. A., Jr.; Peralta, J. E.; Ogliaro, F.; Bearpark, M.; Heyd, J. J.; Brothers, E.; Kudin, K. N.; Staroverov, V. N.; Kobayashi, R.; Normand, J.; Raghavachari, K.; Rendell, A.; Burant, J. C.; Iyengar, S. S.; Tomasi, J.; Cossi, M.; Rega, N.; Millam, N. J.; Klene, M.; Knox, J. E.; Cross, J. B.; Bakken, V.; Adamo, C.; Jaramillo, J.; Gomperts, R.; Stratmann, R. E.; Yazyev, O.; Austin, A. J.; Cammi, R.; Pomelli, C.; Ochterski, J. W.; Martin, R. L.; Morokuma, K.; Zakrzewski, V. G.; Voth, G. A.; Salvador, P.; Dannenberg, J. J.; Dapprich, S.; Daniels, A. D.; Farkas, Ö.; Foresman, J. B.; Ortiz, J. V.; Cioslowski, J.; Fox, D. J. *Gaussian 09*, Revision A.02; Gaussian, Inc.: Wallingford, CT, 2009.

(20) Hsieh, C.-C.; Chen, K.-Y.; Hsieh, W.-T.; Lai, C.-H.; Shen, J.-Y.; Jiang, C.-M.; Duan, H.-S.; Chou, P.-T. *ChemPhysChem* **2008**, *9*, 2221.

(21) (a) Fidder, H.; Knoester, J.; Wiersma, D. A. *J. Chem. Phys.* **1991**, *95*, 7880. (b) Poliakov, E. Y.; Chernyak, V.; Tretiak, S.; Mukamel, S. *J. Chem. Phys.* **1999**, *110*, 8161.

(22) (a) Katan, C.; Tretiak, S.; Werts, M. H. V.; Bain, A. J.; Marsh, R. J.; Leonczek, N.; Nicolaou, N.; Badaeva, E.; Mongin, O.; Blanchard-Desce, M. *J. Phys. Chem. B* **2007**, *111*, 9468. (b) Terenziani, F.; Le Droumaguet, C.; Katan, C.; Mongin, O.; Blanchard-Desce, M. *ChemPhysChem* **2007**, *8*, 723. (c) Katan, C.; Charlot, M.; Mongin, O.; Le Droumaguet, C.; Jouikov, V.; Terenziani, F.; Badaeva, E.; Tretiak, S.; Blanchard-Desce, M. *J. Phys. Chem. B* **2010**, *114*, 3152. (d) Lahankar, S. A.; West, R.; Varnavski, O.; Xie, X.; Goodson, T., III; Sukhomlinova, L.; Twieg, R. *J. Chem. Phys.* **2004**, *120*, 337. (e) Verbouwe, W.; Van der Auweraer, M.; De Schryver, F. C.; Piet, J. J.; Warman, J. M. *J. Am. Chem. Soc.* **1998**, *120*, 1319.

(23) (a) Larson, D. R.; Zipfel, W. R.; Williams, R. M.; Clark, S. W.; Bruchez, M. P.; Wise, F. W.; Webb, W. W. *Science* **2003**, *300*, 1434. (b) Köler, R. H.; Cao, J.; Zipfel, W. R.; Webb, W. W.; Hanson, M. R. *Science* **1997**, *276*, 2039. (c) Denk, W.; Strickler, J. H.; Webb, W. W. *Science* **1990**, *248*, 73. (d) He, G. S.; Markowicz, P. P.; Line, P.-C.; Prasad, P. N. *Nature* **1999**, *415*, 767. (e) Helmchen, F.; Denk, W. *Nat. Methods* **2005**, *2*, 932.

(24) Velusamy, M.; Shen, J.-Y.; Lin, J. T.; Lin, Y.-C.; Hsieh, C.-C.; Lai, C.-H.; Lai, C.-W.; Ho, M.-L.; Chen, Y.-C.; Chou, P.-T.; Hsiao, J.-K. *Adv. Funct. Mater.* **2009**, *19*, 2388.

JP105542Z